Effect of Cluster Ion Analysis Fluence on Interface Quality in SIMS Molecular Depth Profiling†

Christopher Szakal,*,† Steven M. Hues,‡ Joe Bennett,§ and Greg Gillen†

Surface and Microanalysis Science Division, National Institute of Standards and Technology, 100 Bureau Drive, Gaithersburg, Maryland 20899-8371, Micron Technology, Inc., 8000 S. Federal Way, P.O. Box 6, MS 1-717, Boise, Idaho 83707-0006, and SVTC Technologies, 2706 Montopolis Drive, Austin, Texas 78741

Received: May 28, 2009; Revised Manuscript Received: October 2, 2009

Cluster ion beams are being routinely utilized in secondary ion mass spectrometry (SIMS) for molecular depth profiling analyses, including the generation of three-dimensional data sets. Certain sample targets, such as soft organic matrices, often require large analysis ion fluences in order to generate sufficient count rates for pixel-to-pixel contrast. However, in the generation of this data during a SIMS dual-beam experiment, little attention has been given to the effects imparted into a depth-profiled sample merely by acquiring data between sputter erosion cycles. We find that the amount of Bi_n^+ analysis fluence within a dual-beam sputter depth profiling experiment is not negligible and can degrade the interface widths of a high-quality PMMA film on silicon, despite the use of sputter beams such as SF_5^+ and C_{60}^+ to remove accumulated analysis beam-induced damage. These Bi_n^+ fluence levels, which are often needed for generating enough counts in 3D molecular imaging experiments, can degrade the interface to the point where depth profiling information may not truly reflect the concentration of targeted molecules vs depth. This degradation is expected to worsen for multiple organic layer systems, where the accumulation of ion beam-induced damage can increase to levels where depth-resolved chemistry may not be achievable.

Introduction

Secondary ion mass spectrometry (SIMS) is a surface analysis technique in which energetic primary ions are directed at a target of interest, material inherent to the target is desorbed from the topmost layer(s) of the sample, and the ionized fraction of the desorbed material is subsequently analyzed by mass-to-charge ratio. Because of the chemical sensitivity and surface-specific analysis, inorganic samples have often been sputter depth profiled, where the chemical composition of a sample can be elucidated with respect to depth of controlled primary ion beam-induced erosion. More recently, cluster ion sources such as C_{60}^+, SF_5^+, Bi_n^+, Au_n^+, and others have been utilized to varying degrees for the determination of organic chemical composition vs depth.[1–44] Successful molecular depth profiles of simple organic molecules and systems have led to the ability to create three-dimensional chemical maps of much more detailed sample sets, including biological materials and organic molecule stacks.[19,32,36–38,43] However, much of the three-dimensional work is based on the premise that larger primary cluster ions can be used for controlled sample erosion, and well-focused images can be obtained at each depth point with smaller cluster ions that have better focusing properties. Little has been mentioned about the effects of the analysis (imaging) primary beam on the quality of the molecular depth profile. In this work, we show that the effects of the analysis beam on the quality of the molecular depth profiles and the interfaces are not negligible, and care needs to be taken to ensure that the sample is not being significantly modified during the depth profiling process.

Experimental Methods

Instrumentation. Experiments were performed with an IonToF IV time-of-flight secondary ion mass spectrometer (ToF-SIMS) equipped with 5 keV SF_5^+ and 25 keV Bi_n^+ cluster ion sources, an IonToF V ToF-SIMS instrument equipped with 10 keV C_{60}^+/net 20 keV C_{60}^{+2} and 25 keV Bi_n^+ cluster ion sources, and a Cameca 4f magnetic sector SIMS instrument equipped with either 5.5 keV C_{60}^+ or 5.5 keV SF_5^+ net impact energy cluster ion sources.

For ToF-based analyses, experiments were performed in a "dual-beam analysis", where one projectile is used for the sputter eroding of material from the surface in iterative steps (in these experiments either C_{60}^+ or SF_5^+) and another projectile is used for generating secondary ions for mass analysis between each sputter cycle (in these experiments Bi_n^+). In all cases, ion beams are directed at a grounded surface at 45° from the surface normal. Beam currents were measured in a sample stage-embedded Faraday Cup, sufficient for limiting the emission of sputtered secondary particles of all charges. The ion beams were directed into the center of the Faraday Cup using a 1 μm × 1 μm raster for the Bi_n^+ projectiles and a 0 μm × 0 μm raster for the larger cluster projectiles in order to limit any raster-induced effects into the current measurements. Raster areas were calibrated using the pitch spacing of a sample stage-embedded copper grid. Sputter erosion cycles were in a rastered area of 500 × 500 μm^2 and data analysis cycles were in a rastered area of 200 × 200 μm^2, centered within the sputter beam raster area, except for the highest and second-highest Bi_3^+ fluence levels used, in which cases the analysis areas were 50 × 50 μm^2 and 100 × 100 μm^2, respectively. These experimental conditions resulted in focused probes that in no case were higher than about 2% of the raster areas for each beam. Therefore, no significant

† Part of the "Barbara J. Garrison Festschrift".
* Corresponding author. E-mail: cszakal@nist.gov.
† National Institute of Standards and Technology.
‡ Micron Technology, Inc.
§ SVTC Technologies.

10.1021/jp905019x
Published on Web 11/10/2009

deviations in raster size, and hence ion beam fluence, were imparted into the experiment because of the ion beam widths. Sputter fluences for each erosion cycle were 2×10^{13} ions/cm^2 for SF_5^+ and 2×10^{12} ions/cm^2 for C_{60}^+. Additional specifics are denoted in the text and within each figure caption.

For magnetic sector-based experiments, one beam is used for both data acquisition and sputter erosion, and secondary ions are detected as the material is being removed from the surface. Ion beams at 10 keV are directed at a surface with a bias of +4.5 kV, generating a net 5.5 keV impacting ion at an angle of 42.4° from the surface normal. Raster areas were calibrated using the pitch spacing of a sample block-embedded copper grid. Additional specifics are denoted in the text and within each figure caption.

For dual-beam experiments, analysis fluence was directed in an area within the center of the sputter area so that crater edge effects from the sputter beam would be excluded from the data. For single beam experiments, secondary ions are collected through an aperture that limits the detection to species originating from the center of the beam craters for the same reason as noted above.

Sample Preparation. A high-quality film of average mass 495 000 g/mol poly(methyl methacrylate) (PMMA) was spun-cast onto clean silicon at 200 °C and 1000 rpm, and was obtained from Sematech, Inc. The film was confirmed by ellipsometry to be (100.99 ± 0.62) nm in thickness. A SII (Seiko Instruments, Inc.) Nanopics NPX-200 atomic force profiler was used to measure the average rms surface roughness of the film by scanning three separate film locations at 20 μm scan widths and 90 s scan times in the $x-y$ scan mode. Each of the three film locations was dissected into three regions within each 20 μm scan, giving nine total surface roughness measurements resulting in an average rms surface roughness of 1.27 nm. The Nanopics was calibrated vs depth for the corresponding scan area with a 109 nm step height standard (Standard Pattern NPX1STP001) supplied by SII.

Data Analysis. For normalized depth profile data in Figure 1, the interface position was defined as the point where the sum of PMMA and Si signals intersected at 0.50 for each data set. This point was assigned the film thickness value, and assuming a constant sputter rate throughout the PMMA film, was used to convert the x-axis to a depth scale. In such a normalization scheme, the sum of PMMA (overlayer) and Si (substrate) signals are equal to 1 throughout the bulk of the film as well as in the bulk of the silicon substrate. This interface assignment method is identical to the normalization scheme reported elsewhere for a similar system,[9] although it is recognized that others may use different interface assignment methods, each with advantages and disadvantages in the amount of ambiguities imparted into the interface assignment.

For the remainder of the reported depth profile data in Figures 2−4, no normalization procedure was used. However, the sputter rate obtained for each data set from the normalization procedure was used to assign the x axis to a depth scale. The counts measured from each instrument were directly plotted onto each graph in a log vs linear format, uncorrected for primary ion beam current, and the 1/e values were obtained by determining the depth (in nm) for the PMMA fragment ion signal to decay by a factor of e, as explained in the following section.

Results and Discussion

Normalized depth profile data (as described in the Experimental Methods section) and non-normalized molecular depth profile data signals of the characteristic PMMA fragment ion at m/z 69 (corresponding to $C_4H_5O^+$) and the substrate silicon ion at m/z 28 are plotted in Figures 1 and 2, respectively, vs PMMA film depth. In these plots, the effect of interface quality based on 25 keV Bi_3^+ analysis while sputtering each cycle with 5 keV SF_5^+ primary ions is explored as a function of varying Bi_3^+ fluence and constant sputter fluence (2×10^{13} ions/cm^2 in each cycle). The first two profiles of 1.7×10^{11} ions/cm^2 and

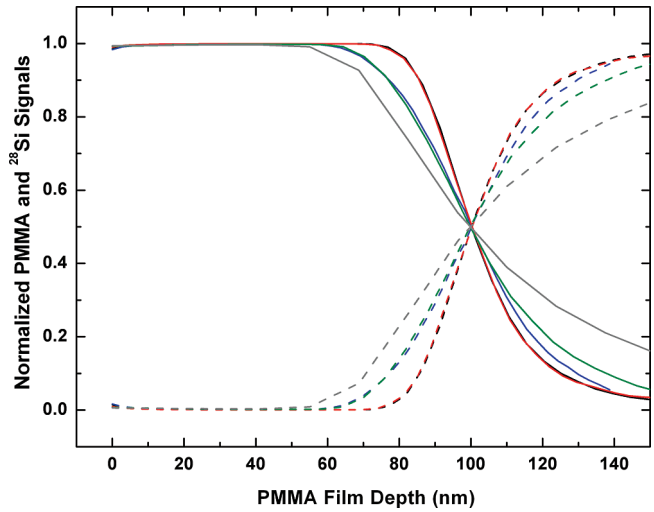

Figure 1. Normalized depth profiles for monitoring the characteristic PMMA fragment ion at m/z 69 (solid lines) and silicon substrate ion at m/z 28 (dashed lines) as a function of total analysis fluence of Bi_3^+ and versus PMMA film depth. Black: 1.7×10^{11} ions/cm^2 Bi_3^+, Red: 4.6×10^{11} ions/cm^2 Bi_3^+, Blue: 2.2×10^{12} ions/cm^2 Bi_3^+, Green: 4.5×10^{12} ions/cm^2 Bi_3^+, and Gray: 8.2×10^{12} ions/cm^2 Bi_3^+. All data was acquired with 5 keV SF_5^+ as the sputter projectile and 25 keV Bi_3^+ as the analysis probe. Fluence levels are totals for analysis fluence in all cycles until the interface is reached. Sputter erosion fluence (2×10^{13} ions/cm^2) in each cycle is larger than the total analysis fluence for each experiment.

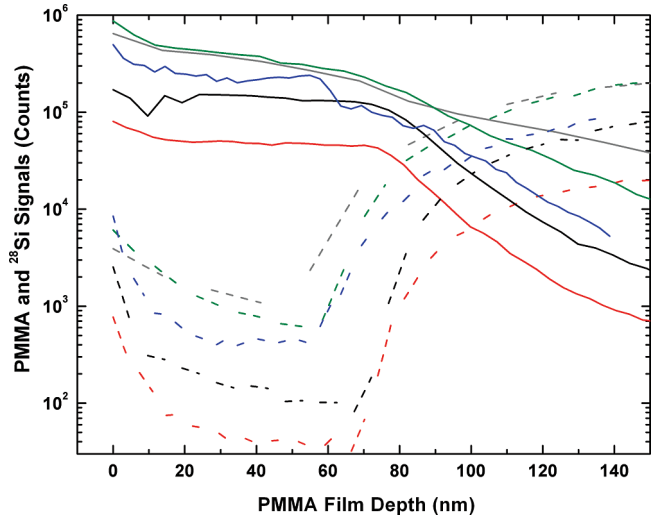

Figure 2. Depth profiles for monitoring the characteristic PMMA fragment ion at m/z 69 (solid lines) and silicon substrate ion at m/z 28 (dashed lines) as a function of total analysis fluence of Bi_3^+ and versus PMMA film depth. These profiles were used for calculating 1/e decay lengths. Black: 1.7×10^{11} ions/cm^2 Bi_3^+, Red: 4.6×10^{11} ions/cm^2 Bi_3^+, Blue: 2.2×10^{12} ions/cm^2 Bi_3^+, Green: 4.5×10^{12} ions/cm^2 Bi_3^+, and Gray: 8.2×10^{12} ions/cm^2 Bi_3^+. All data was acquired with 5 keV SF_5^+ as the sputter projectile and 25 keV Bi_3^+ as the analysis probe. Fluence levels are totals for analysis fluence in all cycles until the interface is reached. Sputter erosion fluence (2×10^{13} ions/cm^2) in each cycle is larger than the total analysis fluence for each experiment.

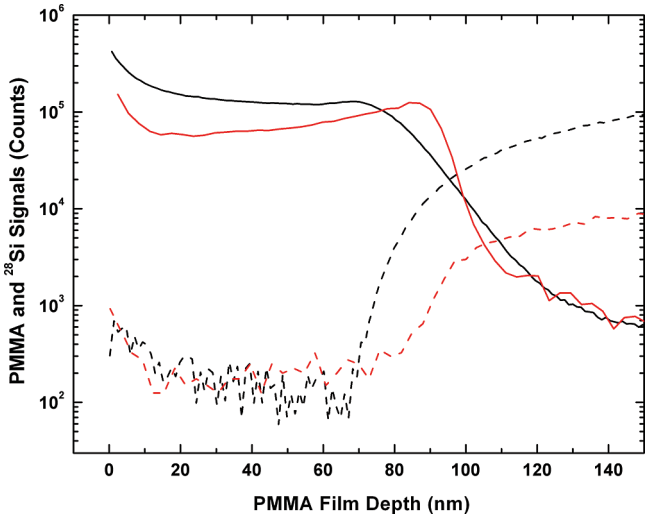

Figure 3. Depth profiles for monitoring the characteristic PMMA fragment ion at *m/z* 69 (solid lines) and silicon substrate at *m/z* 28 (dashed lines) versus PMMA film depth. These profiles were used for calculating 1/e decay lengths. Black: 5.5 keV SF_5^+ sputter and analysis, Red: 5.5 keV C_{60}^+ sputter and analysis. All 1/e decay length data from this plot summarized in Table 1.

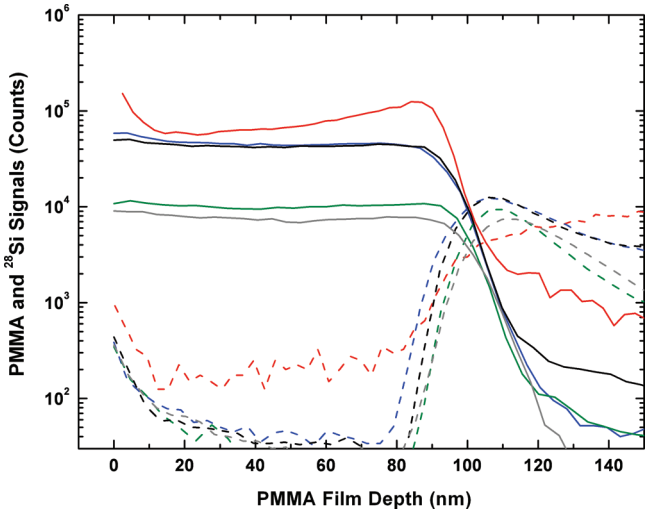

Figure 4. Depth profiles for monitoring the characteristic PMMA fragment ion at *m/z* 69 (solid lines) and silicon substrate at *m/z* 28 (dashed lines) versus PMMA film depth. These data profiles were used for calculating 1/e decay lengths. Red: 5.5 keV C_{60}^+ sputter and analysis from Figure 3, Black: 10 keV C_{60}^+ sputter and 25 keV Bi_3^+ analysis, Blue: net 20 keV C_{60}^{+2} sputter and 25 keV Bi_3^+ analysis, Green: 10 keV C_{60}^+ sputter and 25 keV Bi^+ analysis, and Gray: net 20 keV C_{60}^{+2} sputter and 25 keV Bi^+ analysis. Total Bi_n^+ fluences were kept at the lowest levels of those in Figure 1 and Figure 2 (10^{11} ions/cm^2). All 1/e decay length data from this plot summarized in Table 1.

4.6×10^{11} ions/cm^2 total Bi_3^+ fluence have similar shapes, and the factor of 3 increase in analysis beam fluence did not degrade the profile shape through the polymer/silicon interface. However, increasing total Bi_3^+ analysis fluence further to 2.2×10^{12} ions/cm^2 shows a degradation of the interface and an earlier depth at which silicon signal appears in the profile. Increasing the total Bi_3^+ analysis fluence to the highest values in Figures 1 and 2 (4.5×10^{12} ions/cm^2 and 8.2×10^{12} ions/cm^2) shows a trend of earlier silicon arrival in profile depth to the point where the interface is severely degraded (4.5×10^{12} ions/cm^2 total fluence), and ultimately undeterminable, (8.2×10^{12} ions/cm^2 total fluence). At these high analysis fluence values, Si signals are observed up to 40 nm before the anticipated polymer/silicon interface, which may at first be surprising because of the general surface sensitivity of the SIMS technique but has been seen before for this type of highly energetic, small cluster ion.[45] The cumulative effect of implanting the PMMA film with analysis ions leads to significant degradation of the interface region. The generation of analysis beam-induced topographic roughness can cause channels for substrate ions to eject through the overlayer film en route to mass spectrometric detection. Additionally, the sputter erosion beam may itself induce roughening of the PMMA film based on previously published work,[30] and this fact may play a role in the cumulative ion beam-induced degradation of the PMMA film during a dual-beam experimental approach.

TABLE 1: Summary of Best Possible 1/e Decay Lengths for Depth Profiles of the PMMA Fragment Ion at *m/z* 69 on Silicon

sputter beam/analysis beam	1/e decay length (nm)	1/e data from figure number(s)
5.0 keV SF_5^+/25 keV Bi_3^+	13.1	2
5.5 keV SF_5^+/5.5 keV SF_5^+	10.0	3
5.5 keV C_{60}^+/5.5 keV C_{60}^+	3.9	3 and 4
10.0 keV C_{60}^+/25 keV Bi_3^+	4.8	4
20.0 keV C_{60}^+/25 keV Bi_3^+	4.8	4
10.0 keV C_{60}^+/25 keV Bi^+	5.7	4
20.0 keV C_{60}^+/25 keV Bi^+	7.1	4

The plotted data within both Figure 1 and Figure 2 represent the best possible interface quality profiles for each variable among multiple depth profiles through the PMMA film. For this purpose, the trailing edge signal of the PMMA fragment ion at *m/z* 69 can be simply evaluated for the depth (λ) in which the signal intensity (I) decays by a factor of e (or $I_{\text{depth2}} = I_{\text{depth1}}\, e^{-(\text{depth2-depth1})/\lambda}$).[46] Using this 1/e method for the data plot in Figure 2 to determine these "best-case" interface decay lengths of the PMMA fragment ion profiles, the values generally increase with increasing analysis fluence as follows: 14.1, 13.1, 19.5, 25.6, and 50.5 nm. (The same trend applies for calculating interface widths using the 84%/16% method, which was outlined for polymer samples elsewhere).[3] At first glance, these numbers may not be surprising. As the analysis fluence increases for the highly energetic Bi_3^+ trimer projectile, a significant amount of impact energy is deposited within soft matrices to depths that can exceed 20 nm.[45] The cumulative effect of more subsurface energy deposition with increasing Bi_3^+ analysis fluence may create a more disordered chemistry after bombardment, leading to higher degrees of interlayer mixing and increased topographic roughness, generally developments that preclude the ability to successfully depth profile an organic film. However, the same projectile in this instance is not used for the sputter erosion cycles. By using a larger cluster ion such as SF_5^+, a fraction of the subsurface damage created by the Bi_3^+ projectiles should be removed in each cycle. Certainly the fluence ratio of the "damage removal" projectile to the analysis projectile plays a role in the amount of subsurface damage that can be removed in each cycle. And with constant sputter fluence in this experiment, this ratio is decreasing as the analysis fluence increases. However, even in the scenario where that ratio is near 1×10^3 or 1×10^4, it remains to be seen if the more shallow penetration depths of the larger cluster ions can effectively remove enough analysis beam-induced subsurface damage extending up to 20 nm into the sample and beyond. Additionally, if high analysis fluence levels are required to generate enough ion signals of target molecules, dramatically high sputter erosion fluences would correspondingly be needed to maintain high sputter/analysis fluence ratios, and the ramifications of such an approach are rarely discussed. For example, in order to remove

all subsurface damage created by the analysis beam, combined with the high sputter yields of cluster projectiles, 20−30 nm of material may need to be removed in each cycle in order to avoid cumulative deleterious effects induced by the analysis beam. For thin film analysis, or for complex matrices with multiple concentration gradients, high sputter/analysis ratios will not be ideal for meaningful depth profiling. Hence, the most ideal situation would be where the analysis beam does not impart significant amounts of subsurface damage.

What is not apparent in Figures 1 and 2 is if the relatively small SF_5^+ cluster can efficiently remove enough damage imparted by the Bi_3^+ analysis cycles as compared to larger cluster projectiles used for sputter erosion. In Figure 3, 5.5 keV SF_5^+ projectiles were used for both sputter erosion and analysis, and compared with 5.5 keV C_{60}^+ projectiles for both sputter erosion and analysis. Qualitatively, the SF_5^+/SF_5^+ PMMA depth profile appears similar to the lowest analysis fluence of Bi_3^+ in Figures 1 and 2, where it would be expected that the smallest amount of cumulative damage would be imparted into the film. On initial inspection, the C_{60}^+/C_{60}^+ PMMA depth profile data in Figure 3 can be difficult to compare to the SF_5^+/SF_5^+ data because of the signal spike at the interface. However, compared to the best-case interface decay length of the SF_5^+/Bi_3^+ experiment of 13.1 nm from Figure 2 data, the 1/e decay lengths of the SF_5^+/SF_5^+ and C_{60}^+/C_{60}^+ experiments are 10.0 and 3.9 nm, respectively. Even in the scenario of lowest possible Bi_3^+ analysis fluence for cluster ion depth profiling, there *is* degradation in interface quality when comparing the decay lengths of the SF_5^+/Bi_3^+ and SF_5^+/SF_5^+ depth profiles, as the SF_5^+/SF_5^+ profile results in an improved 1/e decay length. Additionally from the decay length comparison, it is plausible that SF_5^+ is not as efficient at removing accumulated beam-induced physical damage as equal-energy C_{60}^+ projectiles, as the latter profile results in an improved 1/e decay length compared to the SF_5^+ profile. This is possibly related to less cumulative roughening of the PMMA thin film during continued C_{60}^+ bombardment compared to that under SF_5^+ bombardment in a previous study.[30] We can evaluate if this data makes sense, based on the ion beam/solid interactions of the respective cluster projectiles. Both ion beams in the Figure 3 experiment impacted the surface at a net energy of 5.5 keV, giving an average energy of 917 eV/constituent atom for SF_5^+ and 91.7 eV/constituent atom for the C_{60}^+. For the latter, total impacting projectile energy will be much closer to the initial surface than the former, even though both projectiles have properties that are indicative of "damage removal" from previous impacts. This dense region of energy translates to less subsurface mixing and molecular rearrangements for the C_{60}^+ projectile, and as such is a factor for the improved 1/e interface data compared to the SF_5^+ projectile. This energy deposition, in combination with the energy per constituent atom, can also be used to explain the aforementioned PMMA fragment ion signal spike in Figure 3 at approximately 15 nm before the PMMA/Si interface. It is likely that (1) the C_{60}^+ with low net projectile energy implantation depths, is especially sensitive to interface chemistry compared to other projectiles, and due to an imperfectly cleaned silicon substrate that can enhance molecular ionization via the SIMS matrix effect, is a highly surface-sensitive projectile as previously suggested,[45] and (2) the extremely low energy and low mass of each constituent carbon atom can experience recoil from the hard silicon substrate and cause an interface-only enhancement of molecular sputter yield of the overlayer species and, thus, enhancing secondary ion signals in the process. In the Figure 3 experiment, however, each of the two cluster projectiles used were effectively removing ion beam-induced damage as fast as it was created, but the damage was limited since only those cluster beams were employed for both sputter erosion and data analysis.

The data presented in Figure 4 answers the question of whether C_{60}^+ can be efficient at removing Bi_n^+ damage when the Bi_n^+ fluence is kept at the lowest fluence levels of that in Figures 1 and 2 (10^{11} ions/cm^2). Here, the C_{60}-based data from Figure 3 is overlaid with molecular depth profiles of the PMMA film using 10 keV C_{60}^+ sputter projectiles with 25 keV Bi_3^+ and Bi^+ analysis ions, and net 20 keV C_{60}^{+2} sputter projectiles with 25 keV Bi_3^+ and Bi^+ analysis ions. Specifically, the 1/e interface decay lengths for the 10 keV C_{60}^+ profiles are 4.8 and 5.7 nm for 25 keV Bi_3^+ and Bi^+ analysis ions, respectively, and for the net 20 keV C_{60}^{+2} profiles are 4.8 and 7.1 nm for the 25 keV Bi_3^+ and Bi^+ ions, respectively. Additionally, the data in Figure 4 show that the signal spike of the PMMA fragment at the PMMA/Si interface is only present for the data where C_{60}^+ is used for sputter erosion and analysis and is not present when Bi_n^+ ions are use for data analysis. In contrast to the earlier explanation of C_{60}^+ being particularly surface-sensitive, it is believed that the cumulative effect of impacting Bi_n^+ ions would cause enough interlayer mixing where the thin contamination layer at the interface would no longer be a layer, resulting in depth profiles that are less indicative of subtle changes in interface chemistry when analysis projectiles are used that deposit their energy deep beneath the surface.

A summary of all 1/e decay lengths from profile plots in Figures 2−4 is presented in Table 1. The trend of these results where decay lengths decrease with increasing cluster ion size is expected, based on cluster ion characteristic depths of projectile energy loss reported elsewhere.[45] The values in Table 1 for the Bi_n^+/C_{60}^+ profile data show that, if Bi_3^+ is used for data analysis, then there is no statistical difference in the 1/e decay length whether 10 or 20 keV C_{60}^+ is used as the sputter erosion projectile. This may be due to the notion from MD simulations that, with increasing C_{60} energy, impact craters are larger in width, but are relatively the same depth.[47] Experimentally, similar depth profiling interface width data trends were previously reported in work with a Ni:Cr inorganic multilayer stack.[48] The 1/e decay lengths are slightly worse for the Bi^+ atomic projectile compared with the Bi_3^+, which is likely due to a slightly larger energy deposition depth of an impacting monomer compared to a trimer[45] and hence a slightly larger accumulation of subsurface damage. The 1/e values from the Figure 4 experiments using C_{60}^+ as the sputter erosion probe are comparatively lower than those experiments where SF_5^+ was used as the sputter projectile. Recall that even in the experiment where no Bi_n^+ was used, but rather SF_5^+ was used as the sputter *and* analysis beam, the 1/e decay length is about a factor of 2 larger than those with Bi_3^+ as the analysis beam and C_{60}^+ as the sputter probe. This can be attributed to the fact that the SF_5^+ beam itself is imparting some accumulative damage into the PMMA film, and is likely to allow for slight roughening, or "rippling" of the PMMA and/or the silicon as observed previously,[49] whereas this effect is probably not occurring to an appreciable degree in the C_{60}^+ bombardment.

It is important to note that, for reported data from the ToF instrument, the entire analysis area was used for generating the ion signals that were used in each of the depth profile plots. However, at the highest fluence levels, it is conceivable that crater edge effects can be imparted by the analysis beam, which in effect can create an analysis beam-induced crater

within the sputter crater for each depth profile. High-resolution 3D imaging SIMS experiments require high analysis fluence to generate the ion counts per pixel necessary to distinguish areas of chemical localization. Therefore, the reported method of tracking ion signals vs depth is relevant since the analyst would often be interested in the entire image field-of-view. The data reported herein does allow for some approximations of recommended fluence ratios for the different dual-beam depth profiling ion source combinations. With the Bi_n^+ projectiles used for analysis and the SF_5^+ projectiles used for sputter erosion and total Bi_n^+ fluences to the interface in the mid 10^{11} ions/cm^2 as the highest fluence levels before degradation of the interfaces occurred, sputter to analysis fluence ratios of about 1×10^3 would protect the integrity of the interface from accumulated dual-beam degradation. For similar experiments with Bi_n^+ projectiles used for analysis and C_{60}^+ projectiles used for sputter erosion, the sputter to analysis fluence ratios can be about 1×10^2 to protect the integrity of the interface from accumulated dual-beam degradation. It is expected that, in general, the maximum sputter to analysis fluence ratios can be smaller as the analysis and/or sputter projectiles become larger in cluster size, for many of the reasons previously discussed. Additionally, to be complete in data representation, an analysis was completed where only 32% of the pixels of each central analysis area were used for generating ion signals vs depth (for the lowest, highest, and middle Bi_3^+ analysis fluences displayed in Figures 1 and 2). For the original 1/e decay lengths of 14.1, 19.5, and 50.5 nm, these values become 13.9, 17.4, and 24.4 nm when only using the central portions of the analysis fields-of-view for depth profile plot data. At the highest fluence, there is significant deviation in reporting the interface quality when excluding analysis beam-induced crater edge effects. The interface degradation trend remains, however, and the veracity of the notion that increasing analysis beam fluence can degrade the interface quality is proven regardless of the conditions used for data analysis and interpretation.

Conclusions

In conclusion, the data presented herein shows that increasing Bi_n^+ analysis fluence in a dual-beam cluster SIMS molecular depth profiling experiment will degrade the interface quality of a molecular depth-profiled PMMA film on silicon. This data implies that the highly energetic Bi_n^+ projectiles generate enough subsurface molecular damage and/or molecular rearrangement so that cluster erosion projectiles become inefficient at removing the analysis beam-induced effects. For high values of Bi_n^+ analysis fluence (in this particular case, 10^{12} ions/cm^2), which are often needed for generating enough counts for imaging in 3D molecular depth profiling experiments, the interface can become so degraded that depth profiling information may not truly reflect the concentration of targeted molecules vs depth. Additionally, PMMA on Si is a simple system, and it is expected that this behavior will be more pronounced for systems of multiple organic layers where large levels of beam-induced mixing and topographic roughness can accumulate as a function of eroded depth.

Acknowledgment. The authors gratefully acknowledge the NIST Office of Microelectronics Programs for funding of this work. Christopher Szakal recognizes the exemplary career of Dr. Barbara J. Garrison and the profoundly positive impact she has had on both his scientific endeavors and his personal development.

References and Notes

(1) Gillen, G.; Roberson, S. *Rapid Commun. Mass Spectrom.* **1998**, *12*, 1303.
(2) Fuoco, E. R.; Gillen, G.; Wijesundara, M. B. J.; Wallace, W. E.; Hanley, L. *J. Phys. Chem. B* **2001**, *105*, 3590.
(3) Wagner, M. S. *Anal. Chem.* **2004**, *76*, 1264.
(4) Wagner, M. S. *Surf. Interface Anal.* **2004**, *36*, 42.
(5) Wagner, M. S. *Surf. Interface Anal.* **2004**, *36*, 53.
(6) Wagner, M. S. *Surf. Interface Anal.* **2004**, *36*, 62.
(7) Wucher, A.; Sun, S.; Szakal, C.; Winograd, N. *Appl. Surf. Sci.* **2004**, *231*−*232*, 68.
(8) Wagner, M. S.; Gillen, G. *Appl. Surf. Sci.* **2004**, *231*−*232*, 169.
(9) Szakal, C.; Sun, S.; Wucher, A.; Winograd, N. *Appl. Surf. Sci.* **2004**, *231*−*232*, 183.
(10) Wucher, A.; Sun, S.; Szakal, C.; Winograd, N. *Anal. Chem.* **2004**, *76*, 7234.
(11) Wagner, M. S. *Anal. Chem.* **2005**, *77*, 911.
(12) Cheng, J.; Winograd, N. *Anal. Chem.* **2005**, *77*, 3651.
(13) Wucher, A. *Appl. Surf. Sci.* **2006**, *252*, 6482.
(14) Cheng, J.; Winograd, N. *Appl. Surf. Sci.* **2006**, *252*, 6498.
(15) Mahoney, C. M.; Fahey, A. J.; Gillen, G.; Xu, C.; Batteas, J. D. *Appl. Surf. Sci.* **2006**, *252*, 6502.
(16) Conlan, X. A.; Biddulph, G. X.; Lockyer, N. P.; Vickerman, J. C. *Appl. Surf. Sci.* **2006**, *252*, 6506.
(17) Mollers, R.; Tuccitto, N.; Torrisi, V.; Niehuis, E.; Licciardello, A. *Appl. Surf. Sci.* **2006**, *252*, 6509.
(18) Fletcher, J. S.; Conlan, X. A.; Lockyer, N. P.; Vickerman, J. C. *Appl. Surf. Sci.* **2006**, *252*, 6513.
(19) Gillen, G.; Fahey, A.; Wagner, M. S.; Mahoney, C. M. *Appl. Surf. Sci.* **2006**, *252*, 6537.
(20) Aimoto, K.; Aoyagi, S.; Kato, N.; Iida, N.; Yamamoto, A.; Kudo, M. *Appl. Surf. Sci.* **2006**, *252*, 6547.
(21) Mahoney, C. M.; Patwardhan, D. V.; McDermott, M. K. *Appl. Surf. Sci.* **2006**, *252*, 6554.
(22) Conlan, X. A.; Gilmore, I. S.; Henderson, A.; Lockyer, N. P.; Vickerman, J. C. *Appl. Surf. Sci.* **2006**, *252*, 6562.
(23) Mahoney, C. M.; Yu, J.; Fahey, A.; Gardella, J. A., Jr. *Appl. Surf. Sci.* **2006**, *252*, 6609.
(24) Braun, R. M.; Cheng, J.; Parsonage, E. E.; Moeller, J.; Winograd, N. *Appl. Surf. Sci.* **2006**, *252*, 6615.
(25) Baker, M. J.; Fletcher, J. S.; Jungnickel, H.; Lockyer, N. P.; Vickerman, J. C. *Appl. Surf. Sci.* **2006**, *252*, 6731.
(26) Kozole, J.; Szakal, C.; Kurczy, M.; Winograd, N. *Appl. Surf. Sci.* **2006**, *252*, 6789.
(27) Wagner, M. S.; Lenghaus, K.; Gillen, G.; Tarlov, M. J. *Appl. Surf. Sci.* **2006**, *253*, 2603.
(28) Braun, R. M.; Cheng, J.; Parsonage, E. E.; Moeller, J.; Winograd, N. *Anal. Chem.* **2006**, *78*, 8347.
(29) Mahoney, C. M.; Fahey, A. J.; Gillen, G. *Anal. Chem.* **2007**, *79*, 828.
(30) Mahoney, C. M.; Fahey, A. J.; Gillen, G.; Xu, C.; Batteas, J. D. *Anal. Chem.* **2007**, *79*, 837.
(31) Kim, Y. P.; Hong, M. Y.; Kim, J.; Oh, E.; Shon, H. K.; Moon, D. W.; Kim, H. S.; Lee, T. G. *Anal. Chem.* **2007**, *79*, 1377.
(32) Fletcher, J. S.; Lockyer, N. P.; Vaidyanathan, S.; Vickerman, J. C. *Anal. Chem.* **2007**, *79*, 2199.
(33) Hinder, S. J.; Lowe, C.; Watts, J. F. *Surf. Interface Anal.* **2007**, *39*, 467.
(34) Wucher, A.; Cheng, J.; Winograd, N. *Anal. Chem.* **2007**, *79*, 5529.
(35) Zheng, L. L.; Wucher, A.; Winograd, N. *J. Am. Soc. Mass Spectrom.* **2008**, *19*, 96.
(36) Vaidyanathan, S.; Fletcher, J. S.; Goodacre, R.; Lockyer, N. P.; Vickerman, J. C. *Anal. Chem.* **2008**, *80*, 1942.
(37) Jones, E. A.; Lockyer, N. P.; Vickerman, J. C. *Anal. Chem.* **2008**, *80*, 2125.
(38) Fletcher, J. S.; Rabbani, S.; Henderson, A.; Blenkinsopp, P.; Thompson, S. P.; Lockyer, N. P.; Vickerman, J. C. *Anal. Chem.* **2008**, *80*, 9058.
(39) Wucher, A.; Cheng, J.; Winograd, N. *J. Phys. Chem. C* **2008**, *112*, 16550.
(40) Green, F. M.; Gilmore, I. S.; Seah, M. P. *Rapid Commun. Mass Spectrom.* **2008**, *22*, 4178.
(41) Fisher, G. L.; Dickinson, M.; Bryan, S. R.; Moulder, J. *Appl. Surf. Sci.* **2008**, *255*, 819.
(42) Nieuwjaer, N.; Poleunis, C.; Delcorte, A.; Bertrand, P. *Surf. Interface Anal.* **2009**, *41*, 6.

(43) Several articles in Proceedings of the Sixteenth International Conference on Secondary Ion Mass Spectrometry. *Appl. Surf. Sci.* **2008**, *255*, 803.

(44) Shard, A. G.; Rafati, A.; Ogati, R.; Lee, J. L. S.; Hutton, S.; Mishra, G.; Davies, M. C.; Alexander, M. R. *J. Phys. Chem. B* **2009**, *113*, 11574.

(45) Szakal, C.; Kozole, J.; Russo, M. F., Jr.; Garrison, B. J.; Winograd, N. *Phys. Rev. Lett.* **2006**, *96*, 216104.

(46) Wilson, R. G. Stevie, F. A. Magee, C. W., *Secondary Ion Mass Spectrometry: A Practical Handbook for Depth Profiling and Bulk Impurity Analysis*; John Wiley & Sons: New York, 1989; pp 2.1−1.

(47) Postawa, Z.; Czerwinski, B.; Szewczyk, M.; Smiley, E. J.; Winograd, N.; Garrison, B. J. *J. Phys. Chem. B* **2004**, *108*, 7831.

(48) Sun, S.; Szakal, C.; Roll, T.; Mazarov, P.; Wucher, A.; Winograd, N. *Surf. Interface Anal.* **2004**, *36*, 1367.

(49) Gillen, G.; Walker, M.; Thompson, P.; Bennett, J. *J. Vac. Sci. Technol. B* **2000**, *18*, 503.

JP905019X